Eur. Phys. J. C (2025) 85:275
https://doi.org/10.1140/epjc/s10052-025-13946-z

THE EUROPEAN PHYSICAL JOURNAL C

Regular Article - Theoretical Physics

Compact stellar models with quasi-local anisotropy

Shyam Das[1,a], **Bikash Chandra Paul**[2,b], **Iftikar Hossain Sardar**[3,c], **Shyamal Kumar Pal**[4,d]

[1] Department of Physics, Malda College, Malda, West Bengal 732101, India
[2] Department of Physics, North Bengal University, Siliguri, West Bengal 734013, India
[3] Department of Mathematics, Prabhu Jagatbandhu College, Howrah, West Bengal 711302, India
[4] Department of Physics, Bijoy Krishna Girls' College, Howrah, West Bengal 711101, India

Received: 24 October 2024 / Accepted: 15 February 2025

Abstract In this article, we introduce a new compact stellar model by deriving simple, exact analytical solutions to the Einstein field equations in the presence of anisotropy. We focus on an anisotropic star, employing the quasi-local method suggested by Horvat et al. (Class Quantum Gravity 28: 025009, 2011) to describe fluid anisotropy within a spherical symmetry using quasi-local variables, whose values are determined from physics within a very small region around a spacetime point. We then ensure smooth matching between the interior spherically symmetric spacetime and the exterior Schwarzschild spacetime. To confirm the physical validity of our model, we analyze various parameters both analytically and graphically. To further support our solution's applicability to compact stellar objects, we use observational data from the well-known pulsar $4U\,1608-52$ in our graphical analysis.

1 Introduction

Compact objects are objects of interest in astrophysics which can be used to test the theories in high energies. The equation of state of matter in a compact star is unknown, as the conditions inside cannot be recreated on Earth. We use Einstein's general theory of relativity to understand compact objects [2–4]. The left side of Einstein's field equation comes from the geometry it allows, while the right side is based on the interior matter content.When the equation of state of matter is unknown, an alternative approach to understanding the object is by specifying its geometry. The methodology is being employed for a long time to predict the EoS of matter assuming a given geometry [5–7]. Certain compact objects, such as the X-ray pulsar Her X-1, X-ray burster, X-ray sources 4U 1728-34, PSR 0943+10, RX J 185635-3754, 4U 1820-30, and the millisecond pulsar SAX J 1808.4-3658, have estimated masses and radii that differ from predictions of standard neutron star models. Li et al. [8], Bombaci [9], Dey et al. [10,11], Li et al. [12], Kettner et al. [13] analyzed the observed data of the compact objects and predicted that these stars are different from neutron stars and made up of strange quark matter. The compact objects are classified in the strange star (SS) category. Strange stars (SS) typically have matter densities exceeding nuclear matter density, with both their maximum mass and radii smaller than those of neutron stars. However, their compactification factor (ratio of mass to radius) is found more than the neutron stars. For highly compact objects with matter densities typically exceeding nuclear matter density, the properties of matter, especially in the central core, are not well understood, making reliable information about the equation of state (EOS) unavailable. Consequently, an alternative approach was adopted by Mukherjee et al. [14] to study pressure (p) and energy density (ρ) inside the star. The geometry proposed by Vaidya and Tikekar [5] and Tikekar [15] have been considered as a suitable geometry for the 3-space associated with the interior space-time of such configuration. As a result it makes the Einstein's field equations tractable, and a solution can be obtained which leads to physically viable models of super dense stars in equilibrium.

Understanding the matter composition of a compact star requires linking its theoretical model with observational data through the equation of state (EOS), which relates pressure and density. In stellar modeling, the EOS can serve as either an input. One approach assumes a known EOS and uses the Tolman–Oppenheimer–Volkoff (TOV) equations to

[a] e-mail: dasshyam321@gmail.com
[b] e-mail: bcpaul@associates.iucaa.in (corresponding author)
[c] e-mail: iftikar.spm@gmail.com
[d] e-mail: shyamalbkgc@gmail.com

Published online: 12 March 2025

determine the star's structure. By specifying a central energy density or pressure, the equations are solved radially until the pressure becomes zero, revealing the mass and radius. Alternatively, when the EOS is unknown, models may assume the behavior of pressure, density, or mass or adopt a geometric form for the metric potentials. Such alternative methods have been found to be useful for the development of stellar models as shown by Vaidya and Tikeker and Finch-Skea. These solutions can also provide insights into the EOS by defining the pressure–density relationship.

In this context the physical possibility of Vaidya-Tikekar approach have been also discussed by Knutsen [16]. In the relativistic framework, it is thus important to explore an alternative approach suitable for the description of compact SS objects. Accordingly, suitability of the ansatz considered by Tikekar and Thomas [17–19], prescribing 3-pseudo-spheroidal geometry for the 3-space of the interior space-time of compact SS objects studied. In the literature [20] spherically symmetric solution of Einstein's field equation are used to construct stellar model.

There are several reasons why a strange star may not be spherically symmetric, and the pressure may vary in different directions. However, if there is deviation from the spherical symmetry an anisotropic star results. In an anisotropic ultra compact star, Herrera and Santos [21] predicted that it may be possible to exist a star with two different types of pressures, namely, the radial pressure and the tangential pressure which are different incorporating the anisotropy. In the literature a volume of papers appeared where anisotropic fluid sphere configuration has been explored [22–42]. Bondi [43] studied the link between the surface value of the potential with its highest occurring ratio of the pressure tensor to the local density. Mak and Harko [44] obtained an exact stellar model of quark star, using relativistic solutions of a static spherically symmetric anisotropic quark matter distribution. The stellar model is obtained assuming an EoS where radial pressure obey a linear equation of state but the tangential pressure vary differently. An anisotropic star corresponding to the gravitational field equations is found to exist for interior solution satisfying the required general physical condition inside the star.

In compact stellar models, quasi-local anisotropy refers to the variation in principal pressures within a star that depends on the star's local geometry and structure, rather than being uniform throughout. This pressure anisotropy can arise due to several factors, including strong magnetic fields, rotational forces, or phase transitions in the stellar material [45–56]. Quasi-local variables, which capture information from a small region around a spacetime point, are used to develop the equation of state (EoS) for anisotropic fluids in spherical symmetry. Research on quasi-local anisotropic models seeks to clarify how these factors impact the stability, structure, and evolution of compact objects like neutron stars or strange quark stars. By accounting for anisotropic effects, these models offer a more precise view of the internal dynamics and physical properties of such stellar remnants, potentially shedding light on observable characteristics like mass, radius, and surface temperature.

The Quasi-Local EoS is not universally applicable to all compact objects but is particularly suited for anisotropic compact stars, where anisotropy plays a significant role. Its generality depends on the specific assumptions regarding the local matter distribution and geometry of the star. While it has been successfully applied to certain models, its generality would be further validated through comparison with other established anisotropic models, such as those proposed by Bowers-Liang and Herrera-Santos. A broader applicability of the Quasi-Local EoS could be achieved by testing it in different stellar environments, including both static and dynamic cases, as well as in stars with different mass ranges and interior structures. The validity of the Quasi-Local EoS depends on its ability to accurately describe the physical properties and behavior of compact stars. This profile has been shown to yield physically consistent results, particularly when it comes to modeling anisotropic effects in the interior of compact objects. While the Quasi-Local EoS shows promise due to its flexibility and physical consistency, its generality and validity need to be further explored by testing it in various contexts and comparing it with other models. This would provide a more comprehensive understanding of its potential as a tool for modeling compact anisotropic stars.

In the literature a number of stellar models are obtained considering a given geometry [57,58], the present study is different from that of the earlier approach as the form of anisotropy is considered different which can be used to explore the star satisfactorily. Considering an anisotropic star describe by a new form given by Horvat et al. [1] we study the physical features of a star. Earlier, the well-known Quasi-Local (QL) type EoS were taken into account by the authors [59,60] to model the compact stellar structures. When comparing the approach of the Quasi-Local EoS to other anisotropic models in the field, several key differences and similarities emerge in terms of their formulation, applicability, and the physical insights they provide. The Quasi-Local EoS models anisotropic stars by directly linking pressure anisotropy to the star's local geometry, such as compactness and radial pressure. This contrasts with the Tikekar-Vaidya geometries, which focus on a specific geometric configuration, making the Quasi-Local EoS more flexible and applicable to a broader range of anisotropic effects. Unlike the Bowers-Liang model, which provides general solutions with less local constraint, the Quasi-Local EoS incorporates local geometric properties, offering a more physically consistent approach, particularly for addressing variations in pressure and compactness. Similarly, while the Herrera-Santos model emphasizes internal dynamics, the Quasi-Local EoS

provides a more adaptable framework for modeling stars with complex structures, without assuming a specific form for the equation of state. This flexibility makes it a more suitable tool for stars with varying internal properties.

The quasi-local model can be applied to gravastars, which are proposed as alternatives to black holes. The model would describe the anisotropic pressure within the star, especially in the transition from the stable core to the surrounding exotic matter shell. The model can be extended to exotic stars, including boson stars, composed of scalar fields, and dark energy stars, where dark energy dominates the interior. The quasi-local model can account for varying pressure profiles, helping to describe anisotropy within these objects more accurately, particularly for stars with unconventional internal compositions. The model is useful for modelling neutron stars with exotic features, such as quark stars or stars with superfluid cores. It can describe the anisotropic pressure in these high-density environments, making it suitable for stars where the equation of state varies drastically. The quasi-local model can also be adapted to wormholes, objects with exotic structures that challenge traditional black hole theories. The model could help describe the anisotropic pressure in these objects and explore how it affects their stability and interactions with spacetime.

The objective of the present paper is to obtain an exact analytical model for compact stars with anisotropy based on Finch-Skea background geometry [61]. The radial pressure (p_r) is different from the tangential pressure(p_t) and the effect of anisotropy will be probed to study stability of the star.

The quasi-local anisotropy model is primarily designed for static, equilibrium configurations of compact stars, where the pressure and density gradients remain steady over time. While it provides valuable insights into the internal structure and stability of anisotropic stars, its direct application to dynamic scenarios, such as stellar collapse or accretion, is limited. During these dynamic processes, the time-dependent variations in density, pressure, and anisotropy are significantly more complex and require a fully relativistic treatment of evolving spacetime metrics and fluid properties. For such scenarios, anisotropy models would need to be extended to include temporal terms and account for factors like shock waves, intense energy fluxes, and rapidly changing gravitational fields. Although the quasi-local model's adaptability to local physical conditions suggests potential for refinement in dynamic contexts, its current form does not explicitly incorporate the time-dependent behavior essential for describing processes like collapse or accretion.

This paper is organized as follows: in Sect. 2, we discuss the basic Einstein field equations of a compact star corresponding to the anisotropy. In Sect. 3, by considering Finch Skea metric potential corresponds to g_{rr} and using quasi local anisotropy profile for the interior matter distribution the relevant field equations have been solved. We have discussed all the essential physical criteria for a realistic compact model in Sect. 4. The exterior Schwarzschild space-time is matched with the interior solution over the boundary of the star and the corresponding parameters of the model are determined in terms of mass and radius of the star in Sect. 5. In Sect. 6, we have investigated various model parameters like gravitational potential, density, equation of state parameter etc. In Sect. 7, Considering the pulsar $4U$ 1608 52 as a standard source of observational mass and radius data, the developed model has been validated by analyzing the various physical features and conditions with some graphical representations. Several other pulsars are analyzed to validate the proposed model by presenting their physical parameters in tabular form as well as by graphical representation. In Sect. 8, The stability analysis of the model has been confirmed under several conditions. Finally, discussion have been made in Sect. 9.

2 Einstein field equations

We write the line element describing the interior space-time of a spherically symmetric star in standard coordinates $x^0 = t, x^1 = r, x^2 = \theta, x^3 = \phi$ as

$$ds^2 = e^{\nu(r)}(r)dt^2 - e^{\lambda(r)}dr^2 - r^2(d\theta^2 + \sin^2\theta d\phi^2), \quad (1)$$

where $e^{\nu(r)}$ and $e^{\lambda(r)}$ are the radially dependent gravitational potentials to be determined in our model. The stellar interior has matter distribution which has different pressures along radial and transverse directions i.e., anisotropic in nature and the corresponding energy-momentum tensor assumed to be of the form

$$T_{\alpha\beta} = (\rho + p_t)u_i u_j + p_t g_{ij} + (p_r - p_t)\chi_i \chi_j, \quad (2)$$

where ρ is the the energy-density, p_r and p_t, respectively radial and transverse fluid pressures, u^i is the 4-velocity of the fluid and χ^i is a unit space-like 4-vector along the radial direction so that $u^i u_i = -1$, $\chi^i \chi_j = 1$ and $u^i \chi_j = 0$.

The Einstein field equations for the line element (1) can be writen as ($8\pi G = 1$ and $c = 1$)

$$8\pi\rho = \frac{\left(1 - e^{-\lambda}\right)}{r^2} + \frac{\lambda' e^{-\lambda}}{r}, \quad (3)$$

$$8\pi p_r = \frac{\nu' e^{-\lambda}}{r} - \frac{\left(1 - e^{-\lambda}\right)}{r^2}, \quad (4)$$

$$8\pi p_t = \frac{e^{-\lambda}}{4}\left(2\nu'' + \nu'^2 - \nu'\lambda' + \frac{2\nu'}{r} - \frac{2\lambda'}{r}\right), \quad (5)$$

where primes ($'$) denote differentiation with respect to the radial coordinate r.

The pressure anisotropy $(p_t - p_r)$ of the stellar fluid is then

$$\Delta(r) = \frac{e^{-\lambda}}{4}\left(2\nu'' + \nu'^2 - \nu'\lambda' - \frac{2}{r}(\nu' + \lambda') + \frac{4}{r^2}(e^{\lambda} - 1)\right). \tag{6}$$

The system comprises of four equations Eq. (3)–(6) in 5 independent variables, namely e^{λ}, e^{ν}, ρ, p_r and p_t.

The total mass of a star within a radius r of the sphere is defined as

$$m(r) = \frac{1}{2}\int_0^r \omega^2 \rho(\omega) d\omega. \tag{7}$$

3 Developing a novel model

Following Horvat et al. [1] we have used the Quasi-Local (QL) model to describe the quasi local nature of the the anisotropy. This approach stands out due to its flexibility, physical consistency, and compatibility with observational data, making it a powerful tool for investigating stars with complex internal structures. Unlike other EoS models, such as those by Bowers-Liang and Herrera-Santos, the quasi-local model offers a more direct and consistent method, especially when dealing with boundary conditions and local variations in anisotropy. The model's ability to predict such observable characteristics helps deep understanding of compact objects, which are difficult to study directly due to their extreme conditions.

According to this model the quasi-local nature of anisotropy is as following

$$\Delta = (p_t - p_r) = \frac{\beta}{3} p_r (1 - e^{-\lambda}), \tag{8}$$

where β measures the degree of anisotropy inside the matter fluid. The parameter β represents the extent of anisotropy in the quasi-local anisotropy model used for describing compact stars. It determines how the difference between the radial and tangential pressures depends on the compactness $(2m(r)/r)$ and the radial pressure (p_r). A positive β corresponds to configurations where the star's radius and mass increase, creating a more expansive structure. A negative β results in a reduction of the radius and mass, leading to more compact stellar models. Negative values of β enhance the radial stability of quark stars, making it possible for stable configurations to exist even slightly beyond the maximum mass threshold. At the center of the star, the anisotropy vanishes because the compactness reduces to zero. Similarly, at the star's surface, the anisotropy also vanishes since radial pressure drops to zero. The parameter β plays a critical role in understanding how anisotropic pressures influence the structural and stability properties of interacting quark stars, providing insights into their physical behavior under extreme conditions.

To develop a physically reasonable model of the stellar configuration, we assume Finch and Skea [61] metric potential corresponding to g_{rr}

$$e^{\lambda} = 1 + \frac{r^2}{R^2}, \tag{9}$$

where R is the curvature parameter. In literature, Finch and Skea ansatz has been used to develop realistic stellar models by many authors [62–65]. Using Eq. (8) and Eq. (9) we have

$$\Delta = \frac{\beta p_r r^2}{(r^2 + R^2)}, \tag{10}$$

Now to solve the system we assume a particular anisotropic profile given as

$$\Delta(r) = \frac{r^2(b^2 - r^2)}{(r^2 + R^2)^3}, \tag{11}$$

where b is the boundary of the star determined from the condition of vanishing radial pressure across the surface. The selection of anisotropy is particularly intriguing, as it starts at zero at the center, reaches a maximum at some point within the stellar configuration, and then diminishes to zero at the surface. A similar form of pressure anisotropy has been previously explored [66].

Based upon the above assumption we have now the radial pressure profile as

$$p_r(r) = \frac{3(b^2 - r^2)}{\beta(r^2 + R^2)^2}. \tag{12}$$

Clearly from Eq. (12) we can check that $r = b$ is the boundary of the star where radial pressure drops to zero. From Eq. (8) we can have the form of tangential pressure

$$p_t(r) = p_r(r)\left[1 + \frac{\beta r^2}{3(r^2 + R^2)}\right]. \tag{13}$$

On substitution of p_r on the above Eq. (13) we have

$$p_t(r) = \frac{(R^2 - r^2)[3(r^2 + R^2) + \beta r^2]}{\beta(r^2 + R^2)^3}. \tag{14}$$

Now to obtain the functional form of the other metric potential corresponds to g_{tt} coefficient we use the Eq. (4) to obtain

$$\nu' = \frac{r\left(3b^2 + \beta r^2 - 3r^2 + \beta R^2\right)}{2\beta R^2\left(r^2 + R^2\right)}. \tag{15}$$

On integration we have

$$\nu = \frac{\frac{3}{2}\left(b^2 + R^2\right)\log\left(r^2 + R^2\right) + \frac{1}{2}(\beta - 3)\left(r^2 + R^2\right)}{2\beta R^2} + C_1. \tag{16}$$

Finally we can write

$$e^{\nu} = Ae^{\left(\frac{3\left(b^2+R^2\right)\log\left(r^2+R^2\right)+(\beta-3)\left(r^2+R^2\right)}{4\beta R^2}\right)}, \tag{17}$$

where $A(e^{C_1})$ is integration constants will be obtained from the boundary conditions. While comparing the quasi-local model with others, the current approach to study anisotropic stars is more advantageous. The quasi-local model connects anisotropy to compactness and pressure, ensuring it naturally vanishes at the center and surface. Its adjustable parameter β allows control over anisotropy, with positive values leading to larger, less compact stars and negative values enhancing stability.

In comparison, the Herrera-Santos model associates anisotropy with density and pressure gradients, making it adaptable to gradual variations. However, it may require additional conditions to achieve smooth boundary behavior. This model provides insight into the microphysics of anisotropy and produces a wider range of tidal deformabilities. While the quasi-local model is ideal for high-compactness scenarios, the Herrera-Santos model excels in exploring anisotropy influenced by density and pressure changes, making them complementary in their applications.

Finally we now have the matter density, radial pressure, transverse pressure and mass are obtained as

$$\rho = \frac{r^2 + 3R^2}{\left(r^2 + R^2\right)^2}, \tag{18}$$

$$p_r = \frac{3(b^2 - r^2)}{\beta(r^2 + R^2)^2}, \tag{19}$$

$$p_t = \frac{(R^2 - r^2)[3(r^2 + R^2) + \beta r^2]}{\beta(r^2 + R^2)^3}, \tag{20}$$

$$\Delta(r) = \frac{r^2(b^2 - r^2)}{(r^2 + R^2)^3}, \tag{21}$$

$$m(r) = \frac{r^3}{2\left(r^2 + R^2\right)}. \tag{22}$$

4 Essential physical criteria

For a physically viable stellar model, should satisfy the following conditions throughout the stellar configuration:

4.1 Regularity and singularity-free conditions for gravitational potentials and matter variables

The gravitational potentials e^{ν}, e^{λ} and the matter variables ρ, p_r, p_t should be well defined at the center and regular as well as singularity free throughout the interior of the star.

The energy density ρ should be positive throughout the stellar interior i.e., $\rho \geq 0$. Its value at the center of the star should be positive finite and monotonically decreasing towards the boundary inside the stellar interior, mathematically $\frac{d\rho}{dr} \leq 0$.

The radial pressure p_r and the tangential pressure p_t must be positive inside the fluid configuration i.e., $p_r \geq 0$, $p_t \geq 0$. The gradient of the pressure must be negative inside the stellar body, i.e., $\frac{dp_r}{dr} < 0$, $\frac{dp_t}{dr} < 0$. At the stellar boundary $r = b$ the radial pressure p_r should vanish but the tangential pressure p_t may not zero at the boundary.

At the centre both the pressures are equal which means the anisotropy should vanish at the centre, $\Delta(r = 0) = 0$.

The interior metric functions should match smoothly to the exterior Schwarzschild space-time metric at the boundary with radial pressure to vanish at the boundary.

4.2 Energy conditions

For an anisotropic fluid sphere fulfillment of the either of one energy conditions refers to the following inequalities in every point inside the fluid sphere are required:

(1) Weak Energy Condition (WEC): $p_r + \rho > 0$, $\rho > 0$,
(2) Null Energy Condition (NEC): $p_r + \rho > 0$, $p_t + \rho > 0$,
(3) Strong Energy Condition (SEC): $\rho + p_r \geq 0$; $\rho + p_t \geq 0$; $\rho + p_r + 2p_t \geq 0$,
(4) Dominant Energy Conditions (DEC): $\rho \geq p_r$ and $\rho \geq p_t$,
(5) Trace Energy Conditions (TEC) [67,68]: $\rho - p_r - 2p_t \geq 0$.

4.3 Causality condition

Causality condition has to be satisfied for a realistic model i.e. the speed of sound must be smaller than 1 (assuming the speed of light c=1) in the interior of the star, i.e., $0 \leq \frac{dp_r}{d\rho} \leq 1$, $0 \leq \frac{dp_t}{d\rho} \leq 1$.

4.4 Stability conditions

(1) For a stable model, the adiabatic index should be greater than $\frac{4}{3}$.
(2) Herrera [69] cracking method to study the stability of anisotropic stars suggests that a viable model should also satisfy $-1 < v_t^2 - v_r^2 < 0$, where v_r and v_t are it's radial and transverse speed respectively.

5 Exterior spacetime and boundary conditions

The exterior space-time for a not radiating star is empty and is described by the exterior Schwarzschild solution which is

$$ds^2 = -\left(1 - \frac{2m}{r}\right)dt^2 + \left(1 - \frac{2m}{r}\right)^{-1} dr^2 + r^2\left(d\theta^2 + \sin^2\theta d\phi^2\right), \tag{23}$$

where $r > 2m$, m being the total mass of the stellar object.

The interior spacetime metric (1) must be matched to the exterior Schwarzschild spacetime metric Eq. (23) at the boundary of the star. The continuity of the metric functions across the boundary $r = b$ yields

$$e^{\nu}(b) = \left(1 - \frac{2M}{b}\right), \tag{24}$$

$$e^{\lambda}(b) = \left(1 - \frac{2M}{b}\right)^{-1}. \tag{25}$$

The above boundary conditions determine the constants which are

$$R = \frac{b\sqrt{b-2M}}{\sqrt{2M}}, \tag{26}$$

$$A = \left(1 - \frac{2M}{b}\right) e^{-\frac{(\beta-3)\left(b^2+R^2\right)}{4\beta R^2}} \left(b^2+R^2\right)^{-\frac{3\left(b^2+R^2\right)}{4\beta R^2}}. \tag{27}$$

Radial pressure vanishes at a finite value of the radial parameter r, defined as the radius of the star. Hence the radius of the star can be obtained by utilizing the condition $p_r(r = b) = 0$ which is b. In this model we can tune the model parameter β.

6 Physical analysis and constraints on model parameters

1. The gravitational potentials in this model satisfy, $e^{\nu(0)} = A \exp\left(\frac{\frac{3}{2}\left(b^2+R^2\right)\log\left(R^2\right)+\frac{1}{2}(\beta-3)R^2}{\beta R^2}\right) = constant, e^{\lambda(0)} = 1$, i.e., finite at the center ($r = 0$) of the stellar configuration. Also one can easily check that $(e^{\nu(r)})'_{r=0} = (e^{\lambda(r)})'_{r=0} = 0$. These imply that the metric is regular at the center and well behaved throughout the stellar interior.
2. The central density, central radial pressure and central tangential pressure in this case are: $\rho(0) = \frac{3}{R^2}$, $p_r(0) = \frac{3b^2}{\beta R^4}$, $p_t(0) = \frac{3b^2}{\beta R^4}$. All these quantities should be positive. So β must be a positive quantity mathematically, $\beta > 0$.
3. The gradient of energy density, radial pressure and tangential pressure are respectively obtained as:

$$\frac{d\rho}{dr} = -\frac{2r\left(r^2+5R^2\right)}{\left(r^2+R^2\right)^3}, \tag{28}$$

$$\frac{dp_r}{dr} = \frac{6r\left(-2b^2+r^2-R^2\right)}{\beta\left(r^2+R^2\right)^3}, \tag{29}$$

$$\frac{dp_t}{dr} = \frac{2r\left(b^2\left((\beta-6)R^2-2(\beta+3)r^2\right)+(\beta+3)r^4-2\beta r^2R^2-3R^4\right)}{\beta\left(r^2+R^2\right)^4}. \tag{30}$$

The gradient of the density, radial pressure and tangential pressure are negative inside the stellar body and zero at the centre. It is evident from the above equations that at centre ($r = 0$) gradients are zero. This conditions put restriction $\beta < \frac{6b}{(b^2+R^2)^2}$.

4. The radial and transverse velocity of sound ($c = 1$) are obtained as

$$v_r^2 = \frac{dp_r}{d\rho} = \frac{6b^2-3r^2+3R^2}{\beta r^2+5\beta R^2}, \tag{31}$$

$$v_t^2 = \frac{dp_t}{d\rho} = \frac{b^2\left(2(\beta+3)r^2-(\beta-6)R^2\right)-(\beta+3)r^4+2\beta r^2R^2+3R^4}{\beta\left(r^2+R^2\right)\left(r^2+5R^2\right)}. \tag{32}$$

In this model the speed of sound are smaller than 1 in the interior of the star, i.e., $0 \leq \frac{dp_r}{d\rho} \leq 1$, $0 \leq \frac{dp_t}{d\rho} \leq 1$ which has been shown graphically in the next section. We have the following bound $3b^2+3R^2-\beta b^2 < 5\beta R^2$; $6b^2+3R^2 < 5\beta R^2$;

7. Equation of state parameter is given by

$$\omega_r = \frac{p_r}{\rho};\ \omega_t = \frac{p_t}{\rho} \tag{33}$$

To be non-exotic in nature the value of ω should lie within 0 and 1. Therefore, $\frac{b^2}{\beta R^2} \leq 1$ i.e., $\beta \geq \frac{b^2}{R^2}$.

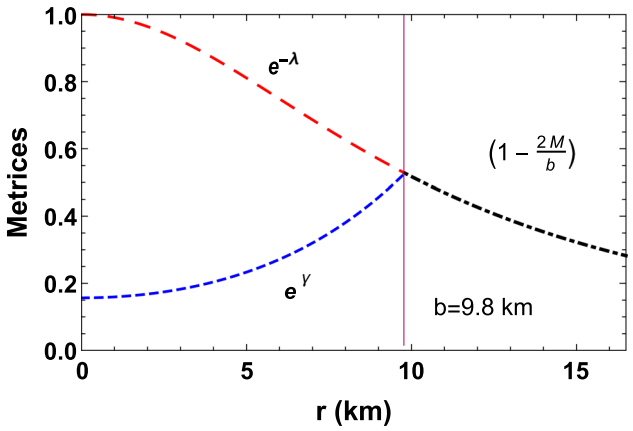

Fig. 1 Matching of the matrices across the surface

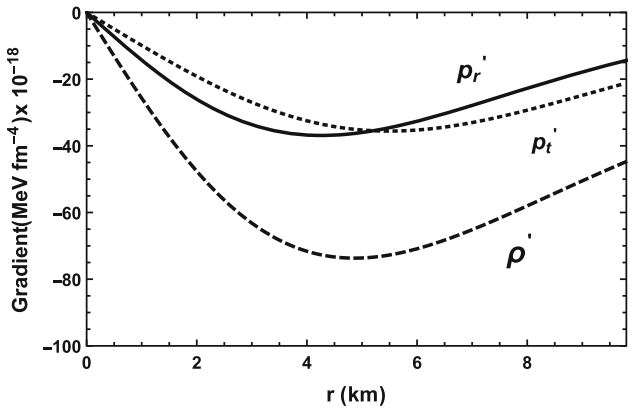

Fig. 2 Gradient

Figure 2 shows the variation of gradients which are negative throughout the stellar configuration except zero at the centre confirms the monotonically decreasing nature of energy density, radial and transverse pressures.

7 Alignment with observational data

7.1 The specific pulsar $4U\,1608-52$

The physical acceptability of this model has been verified by observed values of the masses and radii of pulsars as input parameters. For this purpose, we have considered the pulsar 4U 1608 − 52 having mass = $1.57^{+0.30}_{-0.29}\ M_{\odot}$ and radius = 9.8 ± 1.8 km [70]. Using these values of mass and radius as an input parameter along with $\beta = 3$, the boundary conditions have been utilized to determine the constants as $A = 0.000022174$, $R = 10.352$. Making use of these values of constants and inserting the values of G and c in the expressions, various physical variables have been plotted graphically.

Non singular and well-behaved nature of all the relevant physically meaningful parameters imply that all the requirements of a realistic star are satisfied in this model. Figure 1 depict the regularity and smooth matching of the interior and exterior metrices at the boundary considering the pulsar $4U$ 1608 − 52.

Figure 3 describes the energy density profile in two different visual representations to highlight its spatial variation. Radial Variation representation (left) illustrates the variation of energy density as a function of the radial distance from a central point or origin. The profile typically begins at the center, where the energy density is maximum, and decreases as the distance from the center increases. The contour shading (right) on the right provides a two-dimensional view of the energy density profile.

Variation of radial and tangential pressures has been plotted in Figs. 4 and 5, which are radially decreasing outwards from its maximum value at the center and drops to zero at the boundary. For both figures, the left panel presents a detailed radial perspective, illustrating the variation of pressures as a function of radial distance from a central point. The right panel provides a broader surface or contour analysis, using shading or contour lines to represent the spatial distribution of energy density across a two-dimensional plane.

The radial variation and contour analysis of anisotropy has been shown in the left and right panels of Fig. 6 respectively, which is zero at center and increases to a certain peak near 6 km around, then decreases to zero at the surface.

Figure 7 shows the sound speed in radial and transverse directions remain well below of the given limit to ensure the non-violations of causality condition in the interior of the star.

All the energy conditions are plotted in Fig. 8, which are non-negative throughout the stellar interior as required for a physically realistic star. NEC, WEC, SEC in the left panel and Trace Energy condition (TEC) in the right panel.

The relationship between the thermodynamic parameters energy density and pressure that inferred the nature of the equation of state (EoS) of the matter distribution of this model is plotted in Fig. 9a. The nature shows an non-linear relationship from the best fit curve shown in Fig. 9b. The corresponding best fitted non-linear equation is $p_r = -26.30 + 0.000396092\ \rho^2$.

The mass function is monotonically increases as the function of r and $m(0) = 0$ as shown in Fig. 10.

We can study the effects of the parameter β on the relevant physical parameters in this model. The energy density does not have any effect on the parameter β. On varying the β parameter physical quantities like radial pressure, transverse pressure, EoS are found to vary. As β increases the peak values of radial and transverse pressures shifted to a lower values. Also, EoS gets stiffer as β takes small values. In Figs. 11 and 12 these variations are plotted with β. This

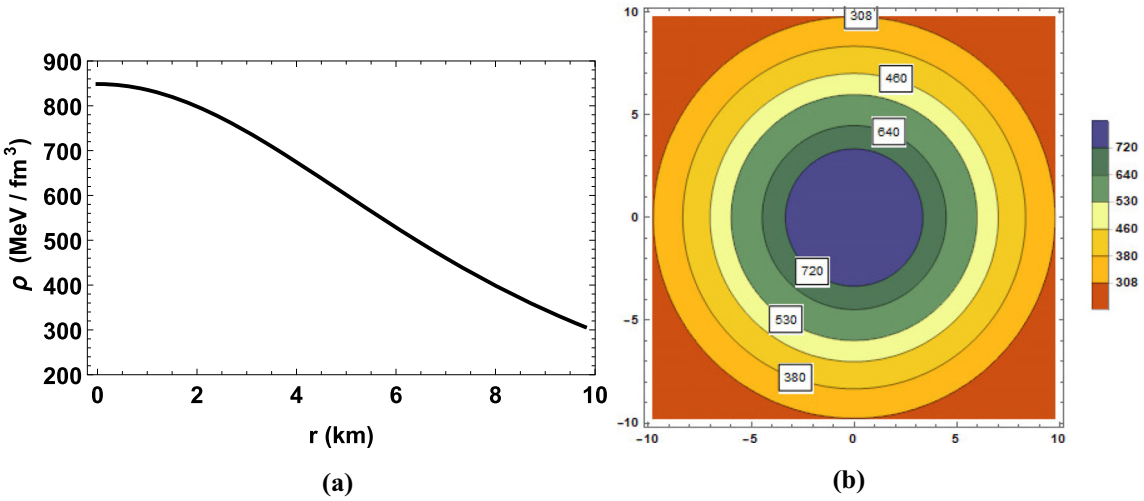

Fig. 3 Energy density profile: **a** radial variation (left), **b** contour shading (right)

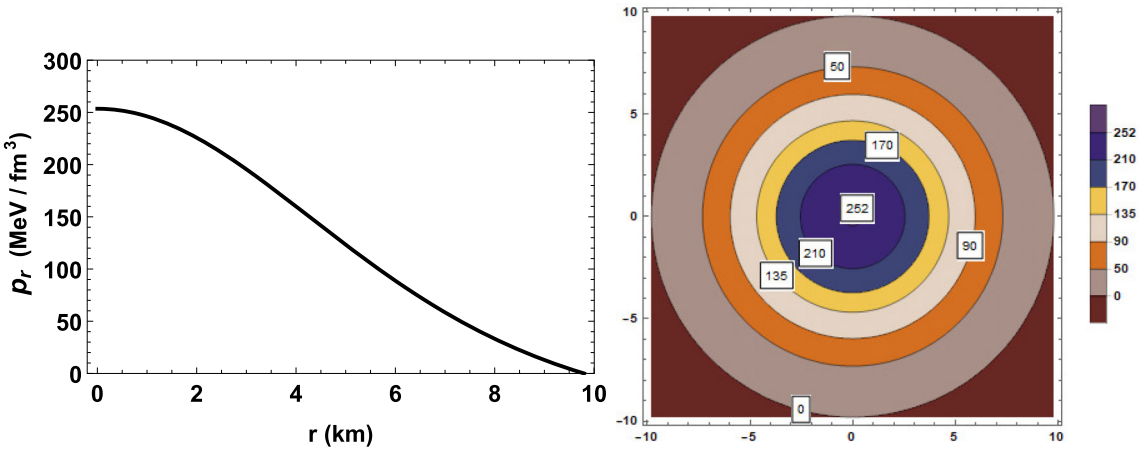

Fig. 4 Radial pressure profile: **a** radial variation (left), **b** contour shading (right)

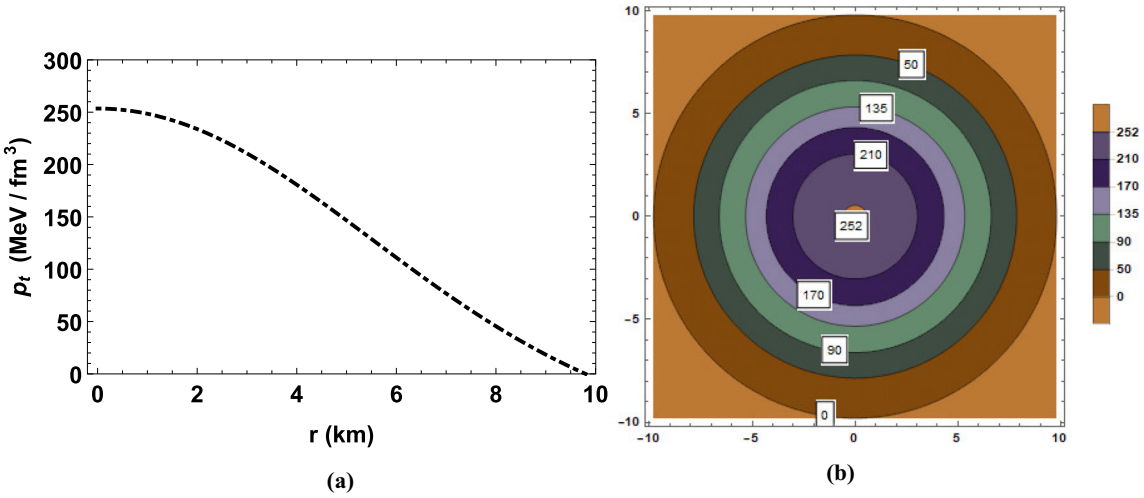

Fig. 5 Transverse pressure profile: **a** radial variation (left), **b** contour shading (right)

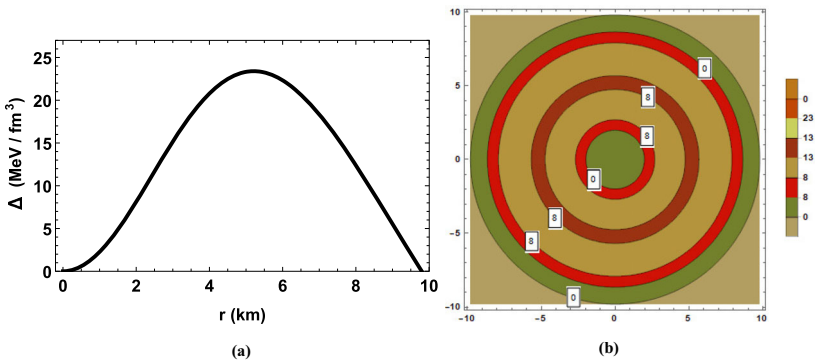

Fig. 6 Anisotropy pressure profile: **a** radial variation (left), **b** contour shading (right)

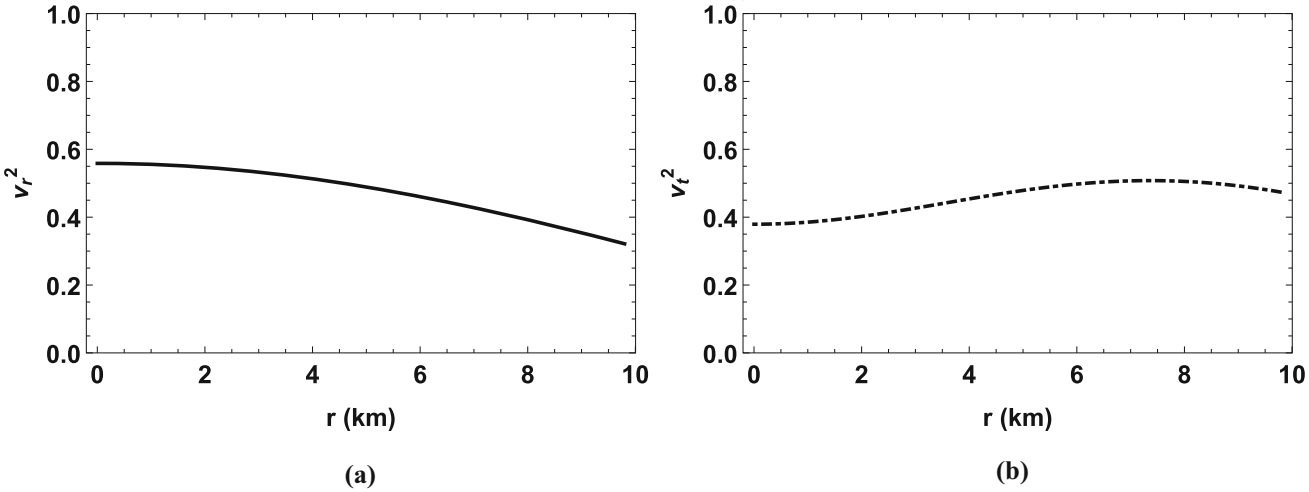

Fig. 7 Sound speed profile: **a** radial (left), **b** transverse (right)

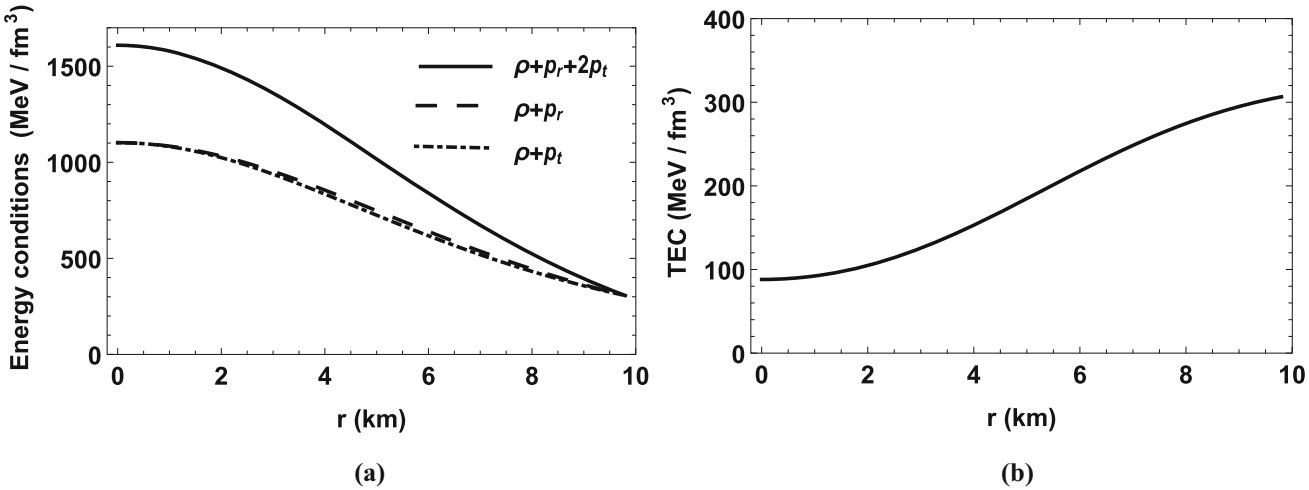

Fig. 8 Energy conditions: **a** NEC, WEC, SEC (left), **b** TEC (right)

ensures the model accurately reflects the behavior of compact stars under extreme conditions and is broadly applicable to various astrophysical scenarios.

Following our model, we have generated the mass–radius ($M-b$) relation assuming the surface density of value $\rho_b = 4.2 \times 10^{14}$ in Fig. 13. Some well-known pulsars, namely SAX J1748.9 − 2021 ($M = 1.81^{+0.25}_{-0.37}\ M_\odot$; $b = 11.7 \pm 1.7$ km), $4U$ 1820 − 30 ($M = 1.46 \pm 0.21\ M_\odot$; $b = 11.1 \pm 1.8$ km), Vela X-1 ($M = 1.77 \pm 0.08\ M_\odot$; $b = 10.654$ km), Her X-1 ($M = 0.85 \pm 0.15\ M_\odot$; $b = 8.1$ km), $4U$ 1608 − 52 ($M = 1.57^{+0.30}_{-0.29}\ M_\odot$; $b = 9.8 \pm 1.8$ km), $4U$ 1724 − 207 ($M = 1.81^{+0.25}_{-0.37}\ M_\odot$; $b = 12.2 \pm 1.4$ km), EXO 1745 − 268 ($M = 1.65^{+0.21}_{-0.31}\ M_\odot$; $b = 10.5 \pm 1.6$ km) and KS 1731−260

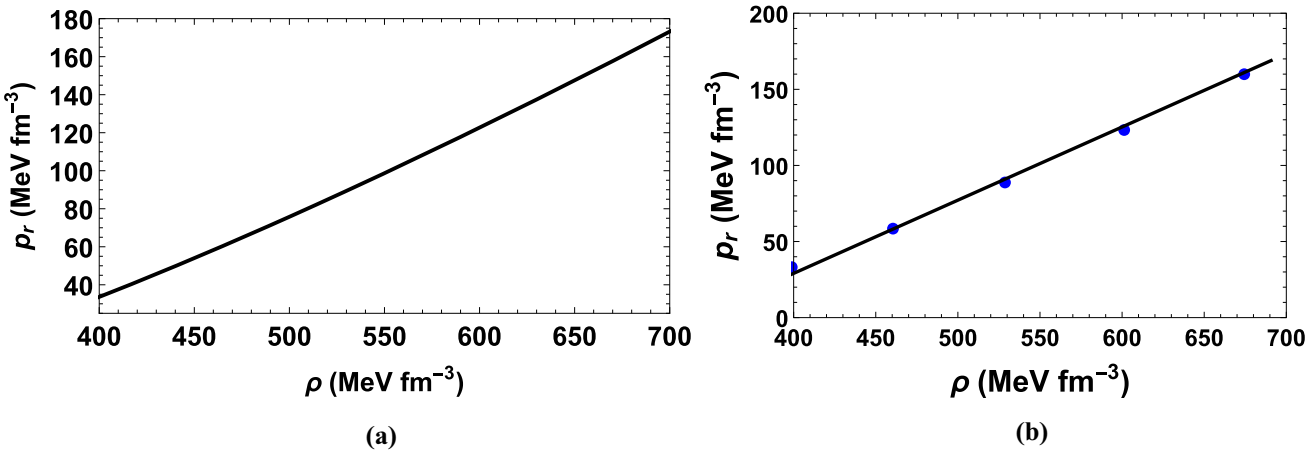

Fig. 9 EoS: **a** nature of profile (left), **b** best fit curve (right)

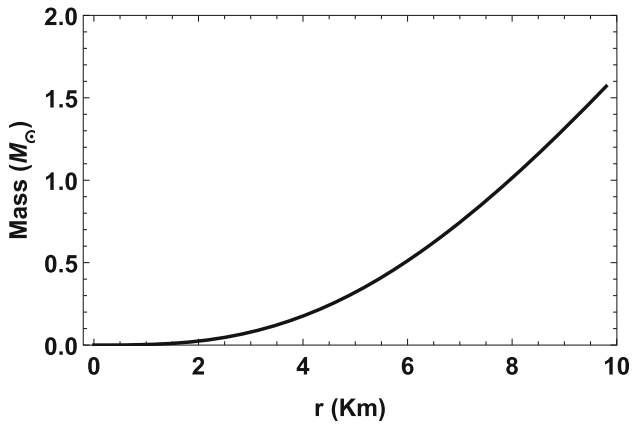

Fig. 10 Mass function

($M = 1.61^{+0.35}_{-0.37}\ M_\odot$; $b = 10 \pm 2.2$ km) are found to predict their masses and radii to a good agreement with our model, as shown in the diagram.

7.2 Additional pulsars as input data

To show that this model has a wide ranges of predictability for compact stars, we have considered some well-known observed pulsars namely, Cen X-3, SAX J 1748.9, Vela X-1, PSR $J0030+0451$, Her X - 1, $KS\ 1731-260$, EXO $1745-268$ and $4U\ 1724-207$.

The measured data corresponding to masses and radii of these pulsars have been used to determine the corresponding model parameters as given in Table 1. Using of these values, in Table 2, we have determined the values of the physically reasonable parameters. All these parameters are sufficient to justify the requirements of a physically realistic star. Here we assign $()|_0$ and $()|_b$ to denote the calculated values of the physical parameters at the center and surface of the star, respectively (Figs. 14, 15, 16).

We use the notation P1=Cen X-3, P2=SAX J1748.9 − 2021, P3=Vela X-1, P4=PSR J0030 + 0451, P5=Her X-1,

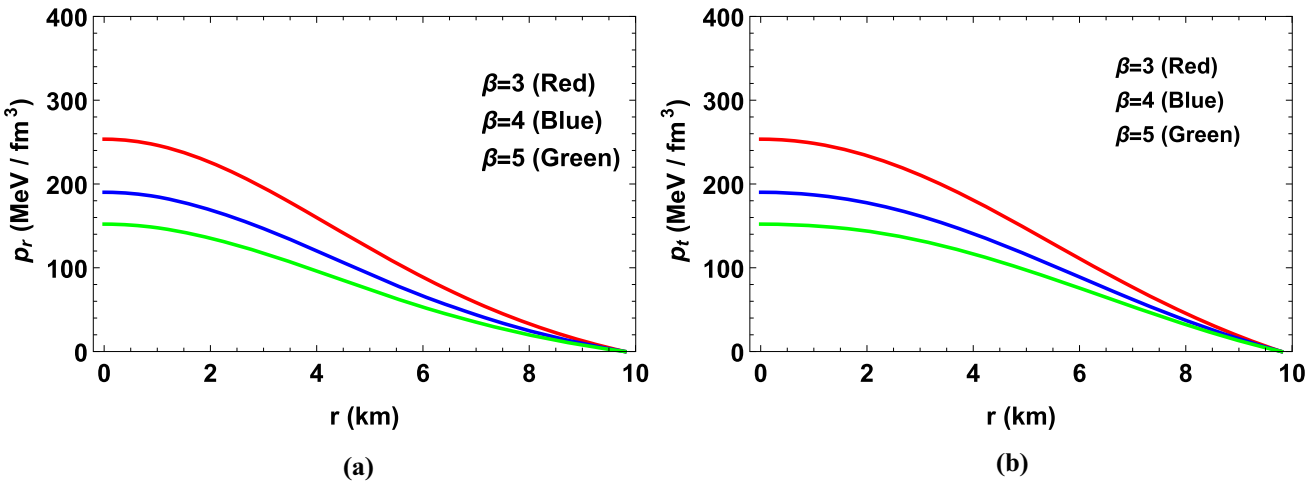

Fig. 11 Variation of pressure with β. **a** Radial pressure (left), **b** transverse pressure (right)

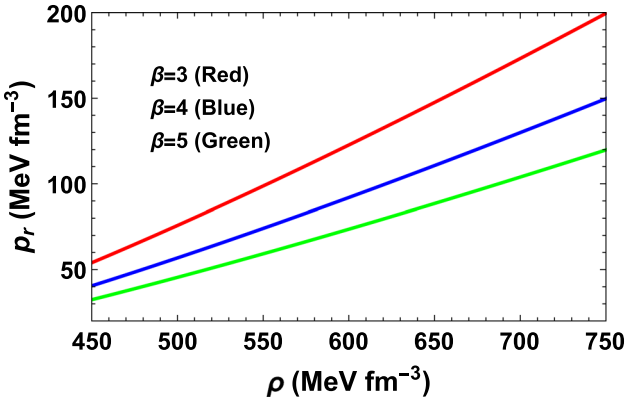

Fig. 12 EoS with β

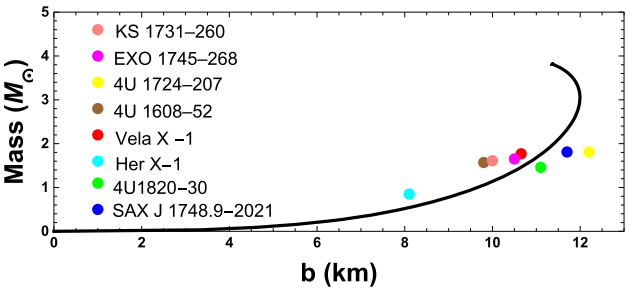

Fig. 13 Mass–radius (M-b) plot

P6=KS $1731-260$, P7=EXO $1745-268$ and P8=$4U$ $1724-207$. Additionally, by including a few more pulsars data as input namely $LMCX-4$, $4U1820-30$, $SMCX-4$, and $GW170817-1$ event, we conducted a detailed graphical analysis that effectively characterizes the physical features of our model. This analysis further validates the model's accuracy and applicability, demonstrating its relevance to real astrophysical systems.We have shown the graphical analysis in Figs. 17, 18, 19, 20, 21, 22, 23, 24, 25, 26 and 27.

8 Model stability assessment

8.1 Tolman–Oppenheimer–Volkoff (TOV) stability analysis

In static equilibrium a star maintain its equilibrium under the combined effects resulting from gravitational force, hydrostatics force and anisotropic force. This condition is mathematically formulated TOV equation given by

$$-\frac{\nu'}{2}(\rho+p_r)+\frac{2}{r}(p_t-p_r)=\frac{dp_r}{dr}. \tag{34}$$

The Eq. (34) can be written as,

$$F_g+F_h+F_a=0, \tag{35}$$

where the simple analytical expression for F_g, F_h and F_a are obtained as:

$$\begin{aligned} F_g &= -\frac{r\left(3b^2+(\beta-3)r^2+\beta R^2\right)\left(3b^2+(\beta-3)r^2+3\beta R^2\right)}{2\beta^2R^2\left(r^2+R^2\right)^3},\\ F_h &= \frac{6r\left(2b^2-r^2+R^2\right)}{\beta\left(r^2+R^2\right)^3},\\ F_a &= (2(b-r)r(b+r))/(r^2+R^2)^3. \end{aligned} \tag{36}$$

The different forces are plotted in Fig. 14 where the positive joint effects of hydrostatics and anisotropic force are counter balanced by the negative gravitational force to keep the system in static equilibrium.

8.2 Adiabatic index

The adiabatic index which is defined as

$$\Gamma=\frac{\rho+p}{p}\frac{dp}{d\rho}, \tag{37}$$

is concerned to the stability of a anisotropic star. The related condition is $\Gamma>\frac{4}{3}$. In Fig. 15, we have plotted Γ_r, Γ_t, γ respectively. clearly, it can be seen from graph that Γ_r and Γ_t are greater than $4/3$ throughout the stellar interior satisfying the stability condition.

Table 1 Model parameters corresponding to different known compact stars

Compact Star	Mass ($M_\odot$)	Radius (km)	β	R	A
Cen X-3 [70]	1.49 ± 0.08	9.17 ± 0.13	5	9.55	0.0006264
SAX J1748.9 − 2021 [70]	$1.81^{+0.25}_{-0.37}$	11.7 ± 1.7	4	12.76	0.0001312
Vela X-1 [70]	1.77 ± 0.08	9.56 ± 0.08	3	8.71	5.688×10^{-6}
PSR J0030 + 0451 [71]	$1.44^{+0.15}_{-0.16}$	$13.02^{+1.24}_{-1.06}$	3	18.70	0.0000627
Her X-1 [70]	$0.85\pm0.15\ M_\odot$	8.1	3	12.09	0.0002950
KS 1731 − 260 [71]	$1.61^{+0.35}_{-0.37}\ M_\odot$	10 ± 2.2	4	10.51	0.0001561
EXO 1745 − 268 [70]	$1.65^{+0.21}_{-0.31}\ M_\odot$	10.5 ± 1.6	4	10.50	0.0001602
$4U$ 1724 − 207 [71]	$1.81^{+0.25}_{-0.37}\ M_\odot$	12.2 ± 1.4	5	13.82	0.0005492

Table 2 Numerical values of the matter variables

Matter Variables	P1	P2	P3	P4	P5	P6	P7	P8
$\rho\|_0$	995	554	1150	257	620	825	715	476
$\rho\|_b$	350	210	350	135	337	295	265	189
$v_r^2\|_0$	0.33	0.4	0.7	0.40	0.37	0.42	0.41	0.30
$v_r^2\|_b$	0.19	0.24	0.38	0.26	0.25	0.24	0.23	0.14
$v_t^2\|_0$	0.16	0.23	0.42	0.29	0.28	0.23	0.38	0.18
$v_t^2\|_b$	0.34	0.38	0.50	0.36	0.34	0.39	0.38	0.32
$\Gamma_r\|_0$	$>\frac{4}{3}$	$>\frac{4}{3}$	$>\frac{4}{3}$	$>\frac{4}{3}$	$>\frac{4}{3}$	$>\frac{4}{3}$	$>\frac{4}{3}$	$>\frac{4}{3}$
$\Gamma_r\|_b$	$>\frac{4}{3}$	$>\frac{4}{3}$	$>\frac{4}{3}$	$>\frac{4}{3}$	$>\frac{4}{3}$	$>\frac{4}{3}$	$>\frac{4}{3}$	$>\frac{4}{3}$
$\Gamma_t\|_0$	$>\frac{4}{3}$	$>\frac{4}{3}$	$>\frac{4}{3}$	$>\frac{4}{3}$	$>\frac{4}{3}$	$>\frac{4}{3}$	$>\frac{4}{3}$	$>\frac{4}{3}$
$\Gamma_t\|_b$	$>\frac{4}{3}$	$>\frac{4}{3}$	$>\frac{4}{3}$	$>\frac{4}{3}$	$>\frac{4}{3}$	$>\frac{4}{3}$	$>\frac{4}{3}$	$>\frac{4}{3}$
$(\rho+p_r+2p_t)\|_0$	1530	920	1850	381	895	1370	1177	688
$(\rho+p_r+2p_t)\|_b$	350	224	350	133	349	297	265	191

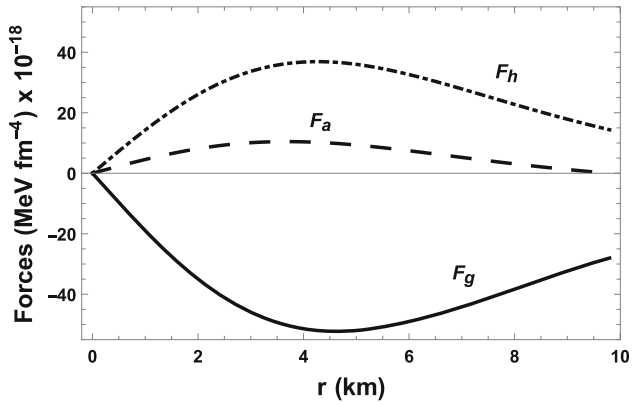

Fig. 14 Contribution of different forces for the static equilibrium of stellar object

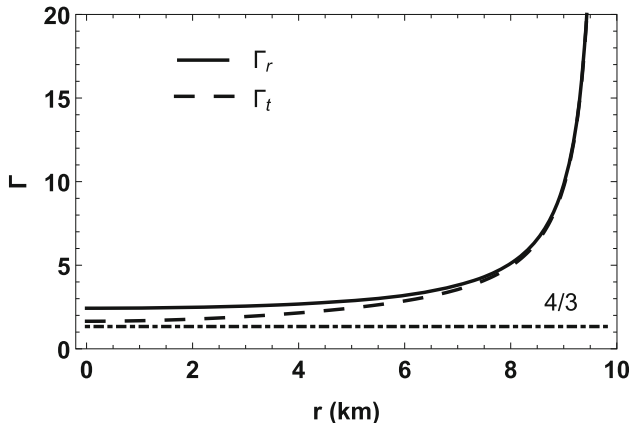

Fig. 15 Adiabatic index

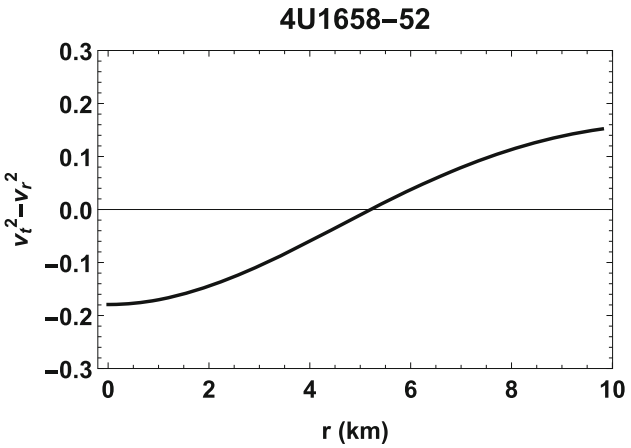

Fig. 16 Difference of sound speeds

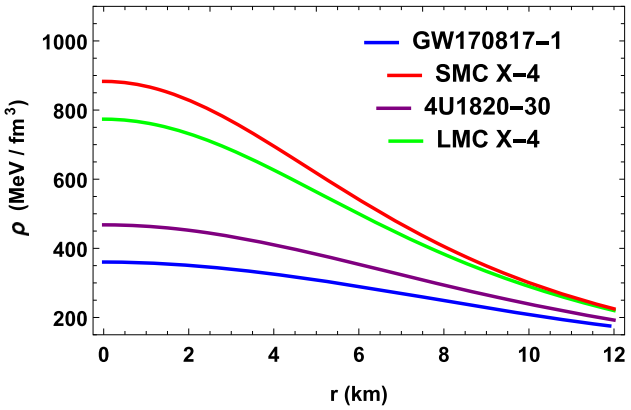

Fig. 17 Radial variation of density for few pulsars

8.3 Herrera's cracking method

Study of cracking method to check the stability of a star was introduced by Herrera [72] where a small perturbation was made from its equilibrium position of a self-gravitating spheres. Latter, Abreu et al. [73] derived a simple mathematical bound on the differences of sound speeds that defines the stability region of a star. It was found that $(v_t^2 - v_r^2 < 1)$ indicated potential stability whereas $(v_t^2 - v_r^2 > 1)$ was unstable. Figure 16 shows that the sound speed stability factor is negative up to a radius 5.5 km.

$$v_t^2 - v_r^2 = \frac{b^2\left(2r^2 - R^2\right) - r^4 + 2r^2R^2}{r^4 + 6r^2R^2 + 5R^4}. \tag{38}$$

Also, the stability factor was independent of the factor β.

9 Discussions

In this paper, we present physically viable solutions to the Einstein field equations for compact stars, meeting essential

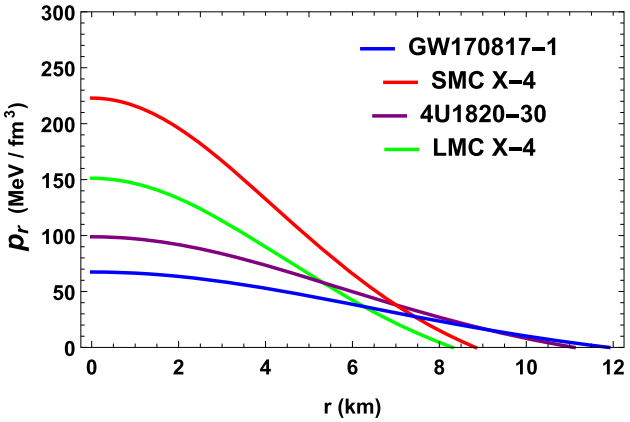

Fig. 18 Radial variation of radial pressure for few pulsars

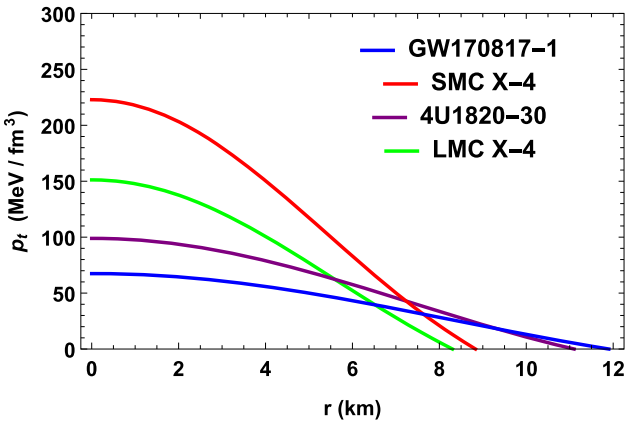

Fig. 19 Radial variation of transverse pressure for few pulsars

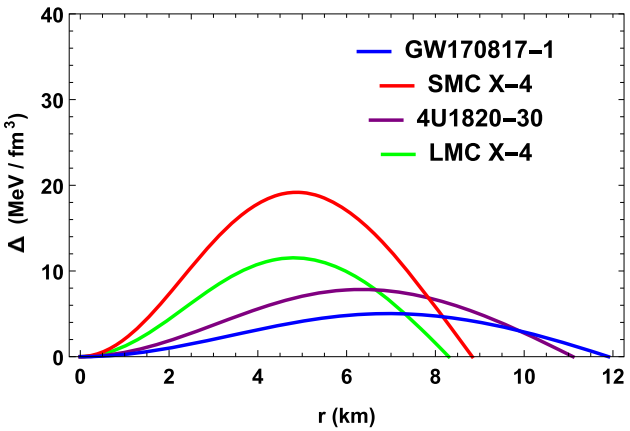

Fig. 20 Radial variation of anisotropy for few pulsars

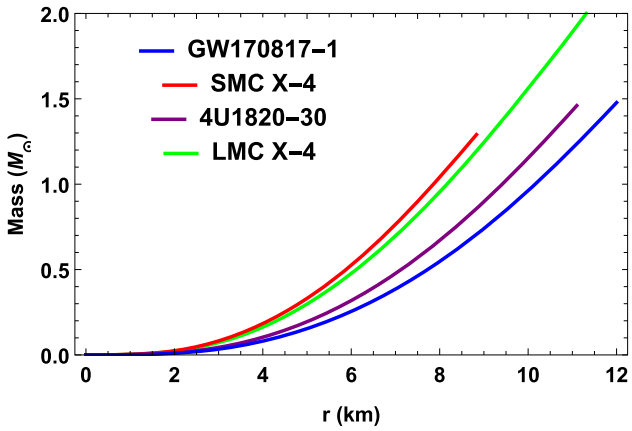

Fig. 21 Radial variation of mass for few pulsars

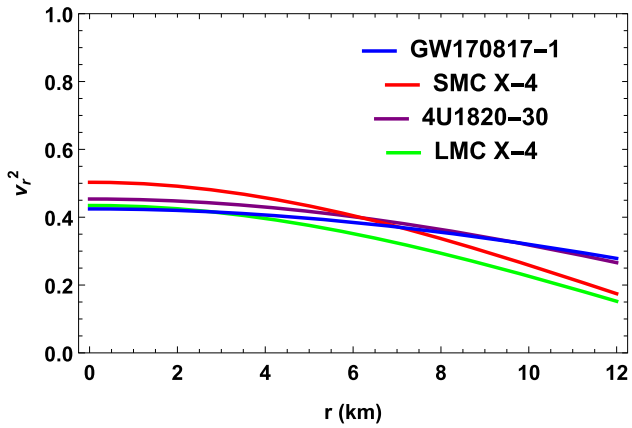

Fig. 22 Radial component of sound speed for few pulsars

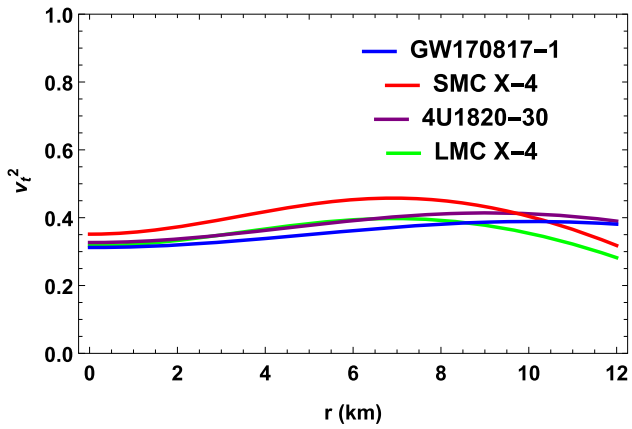

Fig. 23 Transverse component of sound speed for few pulsars

criteria such as the satisfaction of various general relativity energy conditions, subluminal sound speed in the fluid, and, crucially, the stability of the stellar configurations. To model the anisotropic structure of compact stars in spherical symmetry, we adopt a quasi-local equation of state (EoS), which relies on quantities derived from the spacetime geometry at specific points. This quasi-local approach enables us to measure Riemann tensor components in an infinitesimally small region around a point, defining quasi-local variables like the curvature radius and compactness.

The Quasi-Local Anisotropy model provides a flexible framework for incorporating pressure anisotropy to capture deviations from isotropic behavior, which is especially rel-

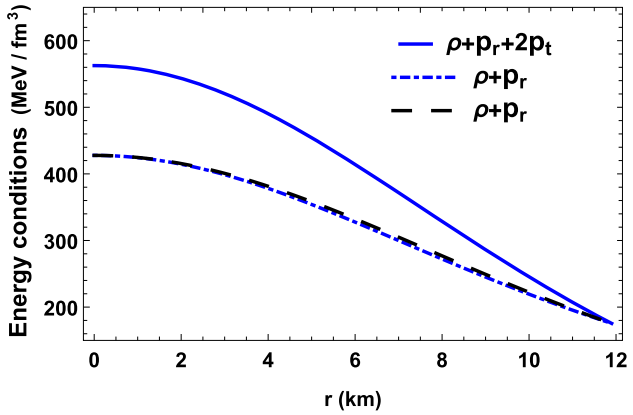

(a) Energy conditions for $GW170817-1$

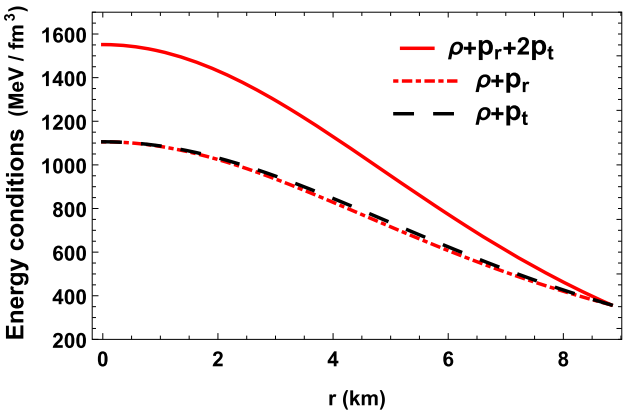

(b) Energy conditions for $SMCX-4$

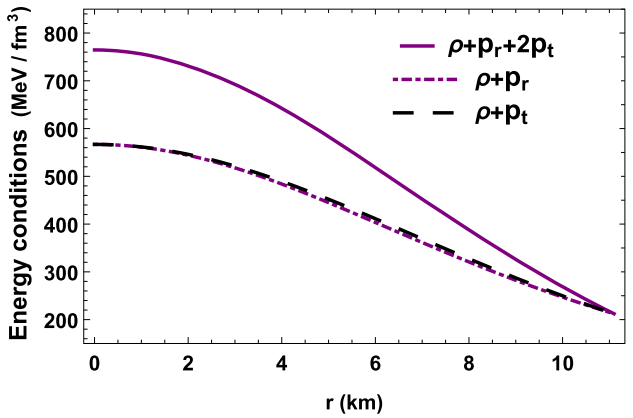

(c) Energy conditions for $4U1820-30$

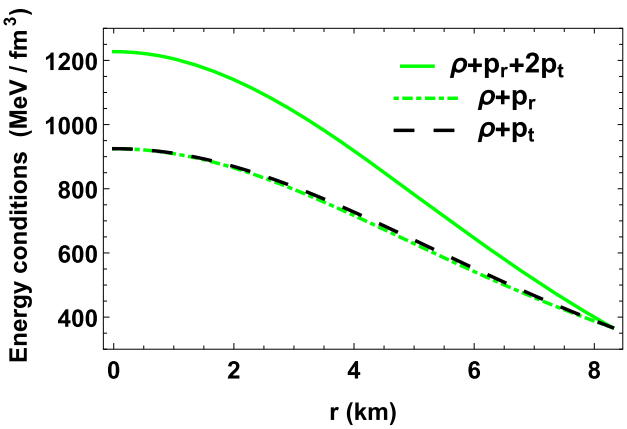

(d) Energy conditions for $LMCX-4$

Fig. 24 Energy conditions for various compact stars

evant for highly dense stellar objects. Unlike conventional approaches that depend on a predefined equation of state (EoS) or assume specific metric potentials, this model naturally accounts for anisotropic stresses and allows macroscopic parameters, such as mass and radius, to serve as inputs. Its versatility makes it particularly well-suited for modeling ultra-compact objects, including neutron stars, strange stars, and highly magnetized stars, where anisotropic pressures are prominent.

Anisotropy is incorporated using a free parameter, denoted as β, which quantifies the level of anisotropy within the stellar structure. The advantage of this quasi-local model is its ability to ensure isotropy at the star's center, while remaining applicable only to relativistic configurations where high densities may induce anisotropy. Our study finds that both radial and transverse pressures depend on β, decreasing as β increases.

The quasi-local EoS offers a unique advantage in modeling anisotropic compact stars as it relates the anisotropic pressure to the local compactness and radial pressure of the star. This ensures that anisotropy vanishes at both the center and surface, which is consistent with physical expectations for such stars. The model adapts to local conditions, providing smooth transitions between the interior and exterior, and includes a free parameter (β), that allows fine-tuning of anisotropy. This EoS has been shown to match well with observational data, including mass–radius relations and tidal deformability measurements, making it valuable for interpreting real astrophysical phenomena. When compared to other models, such as those by Bowers-Liang and Herrera-Santos, the Quasi-Local EoS stands out for its physical consistency, as it directly connects anisotropy to local compactness and pressure, ensuring smooth boundary conditions and offering a more realistic description of stellar structures.

The quasi-local anisotropy model has several cosmological implications, particularly in understanding compact stellar objects and their role in the universe. The quasi-local anisotropy model enhances our understanding of compact stars, gravitational waves, and high-density matter, with

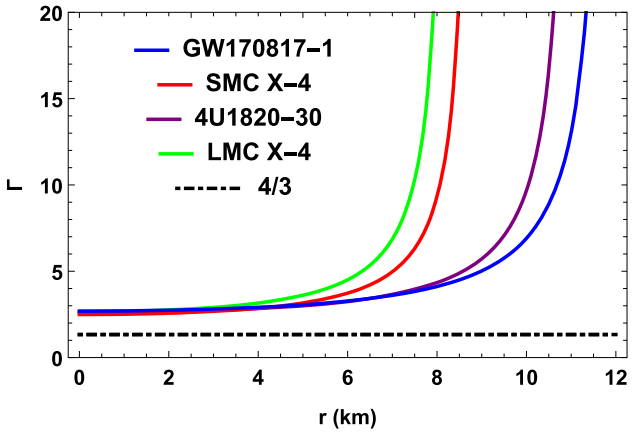

Fig. 25 Variation of Adiabatic Index for few pulsars

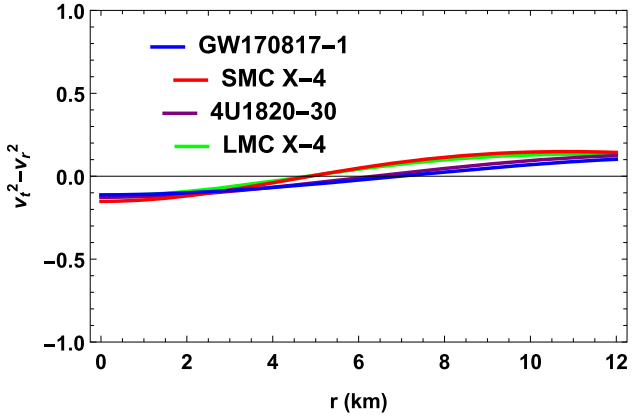

Fig. 26 Difference of sound speeds for few pulsars

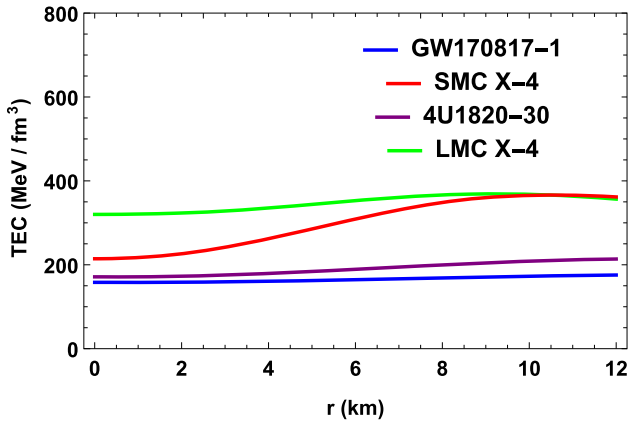

Fig. 27 TEC for few pulsars

broader implications for dark matter, the early universe, and gravitational lensing.

We further demonstrate that the quasi-local EoS allows for the generation of static anisotropic spheres with a broad range of radii and masses, aligning well with recent pulsar measurements. These models are presented on a mass–radius plot, confirming that the quasi-local EoS is a valuable tool for constructing realistic models of compact astrophysical objects, such as neutron stars, that align closely with observational data.

This quasi-local model has certain limitations under which the model might fail. To apply the quasi-local model to exotic objects, modifications are required, such as adjusting equations of state and gravitational field equations for extreme conditions. Additionally, the model doesn't account for anisotropy under dynamic conditions like rotation, magnetic fields, or shock waves. It is also designed for high-density stars and static configurations, making it less suitable for lower-density stars or dynamic processes like collapse or accretion.

However, while our current study focuses on modeling anisotropic pressure in static, spherically symmetric stars, future work will incorporate rotation, magnetic fields, and phase transitions to provide a more comprehensive understanding of compact star.

Acknowledgements S D and BCP gratefully acknowledge support from the Inter-University Centre for Astronomy and Astrophysics (IUCAA), Pune, India, where part of this work was carried out under its Visiting Research Associateship Programme. Shyam Das would also like to express gratitude to ICARD, Malda College.

Data Availability Statement My manuscript has no associated data. [Authors' comment: There are no external data associated with the manuscript.]

Code Availability Statement My manuscript has no associated code/software. [Author's comment: There are no code generated or analysed during the current study.]

Funded by SCOAP^3.

References

1. D. Horvat, S. Ilijic, A. Marunovic, Class. Quantum Gravity **28**, 025009 (2011)
2. C.W. Morris, K.S. Thorne, J.A. Wheeler, *Gravitation* (W.H. Freeman, Princeton University Press, Princeton, 1973)
3. S.W. Weinberg, *Gravitation and Cosmology* (Wiley, New York, 1972)
4. J.V. Narlikar, *An Introduction to Relativity* (Cambridge University Press, Cambridge, 2010)
5. P.C. Vaidya, R. Tikekar, J. Astrophys. Astron. **3**, 325 (1982)

6. R. Tikekar, K. Jotania, Int. J. Mod. Phys. D **14**, 1037 (2005)
7. B.C. Paul, R. Deb, Astrophys. Space Sci. **354**, 421 (2014)
8. X.D. Li, Z.G. Dai, Z.R. Wang, Astron. Astrophys. **303**, L1 (1995)
9. I. Bombaci, Phys. Rev. C **55**, 1587 (1997)
10. M. Dey, I. Bombaci, J. Dey, S. Ray, B.C. Samanta, Phys. Lett. B **438**, 123 (1998)
11. M. Dey, I. Bombaci, J. Dey, S. Ray, B.C. Samanta, Addendum: Phys. Lett. B **447**, 352 (1999)
12. X.D. Li, I. Bombaci, M. Dey, J. Dey, E.P.J. Van Del Heuvel, Phys. Rev. Lett. **83**, 3776 (1999)
13. C. Kettner, F. Weber, M.K. Weigel, N.K. Glendenning, Phys. Rev. D **51**, 1440 (1995)
14. S. Mukherjee, B.C. Paul, N. Dadhich, Class. Quantum Gravity **14**, 3475 (1997)
15. R. Tikekar, J. Math. Phys. **31**, 2454 (1990)
16. H. Knutsen, Mon. Not. R. Astron. Soc. **232**, 163 (1988)
17. R. Tikekar, V.O. Thomas, Pramana J. Phys. **50**, 95 (1998)
18. R. Tikekar, V.O. Thomas, Pramana J. Phys. **52**, 237 (1999)
19. P.K. Chattopadhyay, B.C. Paul, Pramana J. Phys. **74**, 513 (2010)
20. M.C. Durgapal, R. Bannerji, Phys. Rev. D **25**, 328 (1983)
21. L. Herrera, N.O. Santos, Phys. Rep. **286**, 53 (1997)
22. S.D. Maharaj, R. Maartens, Gen. Relativ. Gravit. **21**, 899 (1989)
23. L.K. Patel, N.P. Mehta, Aust. J. Phys. **48**, 635 (1995)
24. M.K. Gokhroo, A.L. Mehra, Gen. Relativ. Gravit. **26**, 75 (1994)
25. S.S. Bayin, Phys. Rev. D **26**, 1262 (1982)
26. M. Cosenza, L. Herrera, M. Esculpi, L. Witten, J. Math. Phys. **22**, 118 (1981)
27. K.D. Krori, P. Bargohain, R. Devi, Can. J. Phys. **62**, 239 (1984)
28. B.W. Stewart, J. Phys. A Math. Gen. **15**, 2419 (1982)
29. T. Singh, G.P. Singh, R.S. Srivastava, Int. J. Theor. Phys. **31**, 545 (1992)
30. G. Magli, J. Kijowski, Gen. Relativ. Gravit. **24**, 139 (1992)
31. G. Magli, Gen. Relativ. Gravit. **25**, 441 (1993)
32. R. Chan, L. Herrera, N.O. Santos, Mon. Not. R. Astron. Soc. **265**, 533 (1993)
33. L. Herrera, P.D. Leon, J. Math. Phys. **26**, 2302 (1985)
34. T. Harko, M.K. Mak, J. Math. Phys. **41**, 4752 (2000)
35. T. Harko, M.K. Mak, Ann. Phys. (Leipz.) **11**, 3 (2002)
36. B.C. Paul, P.K. Chattopadhyay, S. Karmakar, R. Tikekar, Mod. Phys. Lett. A **26**, 575 (2011)
37. P.K. Chattopadhyay, B.C. Paul, in *11th APRIM, 2011 NARIT Conference Series*, Vol. 1, S. Komonjinda, Y. Kovalev, S. Ruffolo (Eds.), p. 258–264
38. B.C. Paul, R. Deb, Astrophys. Space Sci. **354**, 421 (2014)
39. A. Chanda, S. Dey, B.C. Paul, Eur. Phys. J. C **79**, 502 (2019)
40. S. Das, B.C. Paul, R. Sharma, Indian J. Phys. **95**, 2873 (2021)
41. B.C. Paul, S. Das, R. Sharma, Eur. Phys. J. Plus **137**, 525 (2022)
42. B. Das, S. Dey, S. Das, B.C. Paul, Eur. Phys. J. C **82**, 616 (2022)
43. H. Bondi, Mon. Not. R. Astron. Soc. **259**, 365 (1992)
44. M.K. Mak, T. Harko, Chin. J. Astron. Astrophys. **2**(3), 248 (2002)
45. V. Canuto, Ann. Rev. Astron. Astrophys. **12**, 167 (1974)
46. R. Kippenhahn, A. Weigert, *Stellar Structure and Evolution* (Springer, Berlin, 1990)
47. F. Weber, *Pulsars as Astrophysical Observatories for Nuclear and Particle Physics* (IOP Publishing, Bristol, 1999)
48. L. Herrera, N.O. Santos, Astrophys. J. **438**, 308 (1995)
49. P.S. Letelier, Phys. Rev. D **22** (1980)
50. A.I. Sokolov, JETP **79**, 1137 (1980)
51. R.F. Sawyer, Phys. Rev. Lett. **29**, 382 (1972)
52. V.V. Usov, Phys. Rev. D **70**, 067301 (2004)
53. B.V. Ivanov, Int. J. Theor. Phys. **49**, 1236 (2010)
54. F.E. Schunck, E.W. Mielke, Class. Quantum Gravity **20**, R301 (2003)
55. M.S. Morris, K.S. Thorne, Am. J. Phys. **56**, 395 (1988)
56. C. Cattoen, T. Faber, M. Visser, Class. Quantum Gravity **22**, 4189 (2005)
57. Z. Haghani, T. Harko, Phys. Rev. D **107**(6), 064068 (2023)
58. M.I. Wanas, S.A. Ammar, Cent. Eur. J. Phys. **11**, 936–948 (2013)
59. J.M.Z. Pretel, T. Tangphatic, A. Banerjee, A. Pradhan, Phys. Lett. B **848**, 138375 (2024)
60. S.R. Mohanty, S. Ghosh, P. Routaray, H.C. Das, B. Kumar, J. Cosmol. Astropart. Phys. **03**, 054 (2024). https://doi.org/10.1088/1475-7516/2024/03/054
61. M.R. Finch, J.E.F. Skea, Class. Quantum Gravity **6**, 467 (1989)
62. I.H. Sardar, Can. J. Phys. **97**(1), 30–36 (2019)
63. R. Tikekar, V.O. Thomas, Pramana **64**, 5 (2005)
64. R. Sharma, B.S. Ratanpal, Int. J. Mod. Phys. D **13**, 1350074 (2013)
65. D.M. Pandya, V.O. Thomas, R. Sharma, Astrophys. Space Sci. **356**, 285 (2015)
66. P. Bhar, B.S. Ratanpal, Astrophys. Space Sci. **361**, 217 (2016)
67. H. Bondi, Mon. Not. R. Astron. Soc. **302**, 337 (1999)
68. F. Tello-Ortiz, S. Maurya, Y. Gomez-Leyton, Eur. Phys. J. C **80**, 1 (2020)
69. L. Herrera, Phys. Lett. A **165**, 206 (1992)
70. Z. Roupas, G.G.L. Nashed, Eur. Phys. J. C **80**, 905 (2020)
71. M.C. Miller et al., ApJL **887**(1), L24 (2019)
72. R. Chan, L. Herrera, N.O. Santos, Mon. Not. R. Astron. Soc. **267**, 637 (1994)
73. H. Abreu, H. Hernandez, L.A. Nunez, Class. Quantum Gravity **24**, 4631 (2007)